2013-09-20

Blue Light Emitting Electrochemical Cells Incorporating Triazole-based Luminophores

UTD AUTHOR(S): Yulong Shen, Manuel de Anda Villa and Jason D. Slinker

Journal of Materials Chemistry C

RSC Publishing

PAPER

View Article Online
View Journal | View Issue

Blue light emitting electrochemical cells incorporating triazole-based luminophores†

Cite this: J. Mater. Chem. C, 2013, 1, 7440

Jesús M. Fernández-Hernández,‡[a] Sébastien Ladouceur,[b] Yulong Shen,[c] Adriana Iordache,[a] Xiaorong Wang,[b] Loïc Donato,[b] Shawn Gallagher-Duval,[b] Manuel de Anda Villa,[c] Jason D. Slinker,*[c] Luisa De Cola§*[a] and Eli Zysman-Colman*[d]

Received 9th July 2013
Accepted 20th September 2013

DOI: 10.1039/c3tc31307g

www.rsc.org/MaterialsC

We report the electrochemical, photoluminescence, and electroluminescence properties of four fluorinated cationic iridium complexes bearing pyridyltriazole ancillary ligands. All the complexes display unstructured emission in the true blue region at 298 K with photoluminescent λ_{em} ranging from 452 to 487 nm in acetonitrile solution, in powder and in PMMA doped thin films. The nature of the emission is a mixed metal-to-ligand/ligand-to-ligand charge transfer state. Photoluminescence (PL) quantum efficiencies both in solution and in the solid state were low while excited state decay kinetics were found to be multiexponential. Each complex undergoes quasi-reversible oxidation and irreversible reduction with large HOMO–LUMO gaps. A detailed computational investigation corroborates the spectroscopic assignments. Additionally, light-emitting electrochemical cells (LEECs) were fabricated for each of the four complexes. The electroluminescence (EL) spectra of all complexes were red-shifted relative to the PL spectra. The LEEC containing **2a** is the bluest emitter (λ_{max} = 487 nm) of the family of complexes.

Introduction

The current state-of-the-art electroluminescent (EL) devices for visual display and flat panel lighting are organic light emitting diodes (OLEDs). OLEDs possess multilayer architectures typically several hundred nm in thickness that are fabricated using vacuum deposition techniques. The luminophore is typically a small neutral fluorescent organic or phosphorescent organometallic molecule or a polymer. Low work function electrodes are required thus necessitating encapsulation of the device to isolate it from ambient environmental conditions. These limitations drive up the cost of production of OLEDs.

Light-emitting electrochemical cells (LEECs), first reported by Pei and co-workers,[1] are also flat EL devices typically composed of a thin film of a luminescent ionic transition metal complex (iTMC) sandwiched between a semitransparent anode such as indium tin oxide (ITO) and a high work function air-stable cathodes such as Al or Au and can be driven at much lower operating bias than OLEDs. LEEC devices may be formed from solution resulting in easy fabrication and decreased manufacturing costs.[2] Their operation is independent of the work function of the electrodes, rendering the use of less reactive metals as electrodes possible.[3] Due to this, LEECs can uniquely form large area cascaded panels in which the anode of one device serves as the cathode for the next device.[4] Despite all these encouraging features, several challenges remain, such as stability and lifetime of the devices, slow turn on voltage and suitable materials for blue and deep blue emitting LEECs, which will be important for both display and white-light applications.[5]

The luminophoric materials that have received the greatest attention are cationic iridium(III) complexes of the form $[Ir(C^N)_2(N^N)]PF_6$, where C^N is an anionic cyclometallating ligand (*e.g.*, 2-phenylpyridine, ppy) and N^N is a neutral diimine ancillary ligand (*e.g.*, 2,2′-bipyridine, bpy). Their success is due to their desirable photophysical behavior: their phosphorescence with rather short excited state lifetimes (τ_e) and high PL

[a]Westfalische Wilhelms-Universität Münster, Center for Nanotechnology (CeNTech), Heisenbergstrasse 11, 48149 Münster, Germany

[b]Département de Chimie, Université de Sherbrooke, 2500 Boul. de l'Université, Sherbrooke, QC, J1K 2R1, Canada

[c]Department of Physics, The University of Texas at Dallas, 800 W. Campbell Rd, Richardson, TX, USA 75080

[d]School of Chemistry, University of St Andrews, St Andrews, Fife, KY16 9ST, UK. E-mail: ezc@st-andrews.ac.uk; Web: http://www.zysman-colman.com; Fax: +44-(0)1334 463808; Tel: +44-(0)1334 463826

† Electronic supplementary information (ESI) available: ^{1}H and ^{19}F{^{1}H} spectra for complexes. UV-vis and emission spectra at 298 K in ACN solution and 77 K in 2-MeTHF for each complex. Emission spectra of powder samples and thin films for complexes. Cyclic voltammograms for all complexes. Supplementary computational output, including MO quantifications, UV-vis spectra predictions, ground and excited state dipole moment predictions and full TDDFT singlet output for all complexes. See DOI: 10.1039/c3tc31307g

‡ Current address: Grupo de Química Organometálica, Departamento de Química Inorgánica, Facultad de Química, Universidad de Murcia, Apdo. 4 021, 30071 Murcia, Spain.

§ Current address: Institut de Science et d'Ingénierie Supramoléculaires (I.S.I.S.), Université de Strasbourg, 8, allée Gaspard Monge, 67000 Strasbourg, France.

quantum yields (Φ_{PL}), along with facile color tuning mediated through decoration of the organic ligand scaffold. Strategies to obtain blue emission focus on decorating the C^N ligand with electron-withdrawing groups such as fluorine and/or adorning electron-donating groups on the N^N ligand. We have recently shown that replacement of the pyridine ring of the C^N ligand with a 1,2,3-triazole promotes a blue-shift in emission.[6] Moreover, replacement of the bpy ligand for a pyridyl-1,2,3-triazole (pytl) also results in a high energy emission.[7] In this report, we combine these two structural features towards the generation of true blue-emitters for solid-state lighting applications. We show that complexes **1a–2b** (Chart 1) are deep blue emitters in acetonitrile (ACN) solution and in powder as well as in PMMA-doped thin films. We further demonstrate blue-emission in EL devices. We compare the impact of different degrees of fluorination and the effect of *N*-alkylation of the pytl moiety on the optoelectronic properties of the complexes. We rationalize their photophysical behavior through a comprehensive computational study.

Experimental section

General procedures

Commercial chemicals were used as supplied. All experiments were carried out with freshly distilled anhydrous solvents obtained from a Pure Solv™ solvent purification system from Innovative Technologies except where specifically mentioned. Triethylamine (Et_3N) and diisopropylamine (iPr_2NH) were distilled over CaH_2 under a nitrogen atmosphere. Solvents employed for the Click reaction were used without further purification: these consisted of commercial lab grade methanol and deionized water, which was accessible in house.

All reactions were performed using standard Schlenk techniques under an inert (N_2) atmosphere, save for the Click reactions. Flash column chromatography was performed using silica gel (Silia-P from Silicycle, 60 Å, 40–63 μm). Analytical thin layer chromatography (TLC) was performed with silica plates with aluminum backings (250 μm with indicator F-254). Compounds were visualized under UV light. ^1H and ^{19}F NMR spectra were recorded on either a Bruker Avance spectrometer at 400 MHz or a Bruker Avance spectrometer at 300 MHz. The following abbreviations have been used for multiplicity assignments: "s" for singlet, "d" for doublet, "t" for triplet, "m" for multiplet, and "br" for broad. Deuterated chloroform ($CDCl_3$) was used as the solvent of record except where noted below. Spectra were referenced to the solvent peak for ^1H NMR or to $CFCl_3$ for ^{19}F NMR. GC-MS samples were separated on a Shimadzu HP5-MS 30 m × 0.25 mm ID × 0.25 μm film thickness column. Exact mass measurements were performed on a LC-MSD-TOF instrument from Agilent Technologies or on a Bruker Daltonics (Bremen, Germany) MicroTof with loop injection, both in positive electrospray mode. Molecular ions (M^+) were used for empirical formula confirmation. Spectra were recorded either at the Université de Montréal Mass Spectrometry facility in Montréal, Canada or Westfälische Wilhelms-Universität, in Münster, Germany. Elemental analyses were carried out with Carlo Erba 1106 and LECO CHNS-932 microanalyzers.

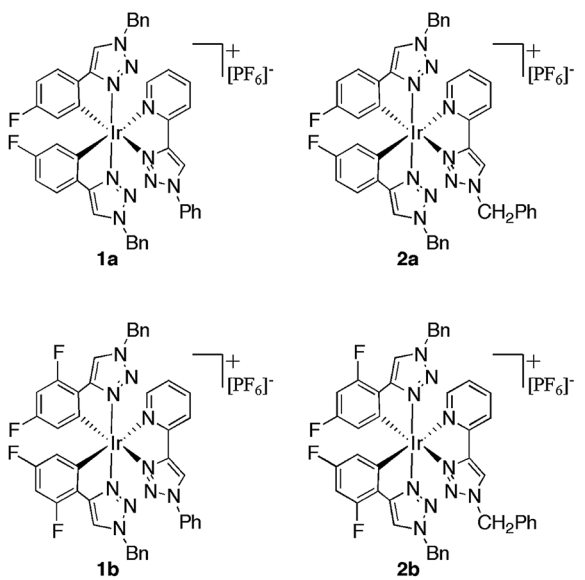

Chart 1 Chemical structures and abbreviations of the complexes investigated.

Synthesis of ligands

The ligands 1-benzyl-4-(2,4-difluorophenyl)-1*H*-1,2,3-triazole (dFphtl), 1-benzyl-4-(4-fluorophenyl)-1*H*-1,2,3-triazole (Fphtl) and 2-(1-benzyl-1*H*-1,2,3-triazol-4-yl)pyridine (pytlBn) were synthesized according to procedures from the literature[8] and the characterization for these compounds matched the literature data.[8,9] The ligand 2-(1-phenyl-1*H*-1,2,3-triazol-4-yl)pyridine (pytlPh) was synthesized and characterized according to a reported procedure.[7]

Synthesis of complexes

Method A. This protocol proceeds *via* isolation of the iridium(III) dimer described by Nonoyama[10] according to the procedure reported by De Cola *et al.* followed by its cleavage with 2 equiv. of the ancillary N^N ligand.[6a] The desired complex was obtained as its PF_6 salt after anion metathesis using NH_4PF_6. This protocol was used for the synthesis of complexes **1a** and **1b**.

The corresponding C^N ligands (0.58 mmol, 2.2 equiv.) and $IrCl_3$ (0.27 mmol, 1.0 equiv.) were placed in a mixture of 2-$EtOCH_2CH_2OH$ and H_2O (6/1) for a concentration of *ca.* 0.04 M of $IrCl_3$. The suspension was degassed repeatedly and placed under N_2 and heated at 110 °C for *ca.* 19 h. The suspension was cooled to room temperature, filtered and the solid obtained was washed with water. The corresponding dimer was used without further purification.

The desired dimer (0.14 mmol, 1.00 equiv.) was suspended in ethylene glycol, to obtain a concentration of *ca.* 0.04 M of dimer, together with the desired N^N ligands (0.30 mmol, 2.2 equiv.). The suspension was degassed repeatedly and placed under N_2 and heated at 150 °C for *ca.* 19 h. The colored solution was left to cool to RT, diluted with water and the resulting

aqueous phase was washed with portions of Et_2O. The aqueous phase was then heated to 70 °C for *ca.* 10 min to remove trace Et_2O and then cooled to RT. To the reaction mixture was added an aqueous solution of NH_4PF_6 (10 mL, 6.13 mmol; 1 g/10 mL) with the subsequent formation of a precipitate. Each complex was purified by flash chromatography on silica gel using a gradient of dichloromethane (DCM) in acetone (0–10%). The purified complex was redissolved in a minimum amount of MeOH and precipitated again by adding it to an aqueous NH_4PF_6 solution (10 mL; 1 g/10 mL). The title complex was filtered, washed with water and dried under vacuum.

Method B. This protocol does not require dimer isolation.[6b] The desired complex was obtained as its PF_6 salt after anion metathesis using NH_4PF_6. This protocol was used for the synthesis of complexes **2a** and **2b**.

The corresponding C^N ligands (0.58 mmol, 2.2 equiv.) and $IrCl_3$ (0.27 mmol, 1.0 equiv.) were placed in a mixture of 2-$EtOCH_2CH_2OH$ and H_2O (6/1) for a concentration of *ca.* 0.04 M of $IrCl_3$. The suspension was degassed repeatedly and placed under N_2 and heated at 110 °C for *ca.* 19 h. The corresponding N^N ligand (0.30 mmol, 1.1 equiv.) was then added and the solution was stirred at 110 °C for *ca.* 19 h. The colored solution was left to cool to RT, diluted with water and the resulting aqueous phase was washed with portions of Et_2O. The aqueous phase was then heated to 70 °C for *ca.* 10 min to remove trace Et_2O and then cooled to RT. To the reaction mixture was added a solution of aqueous NH_4PF_6 (10 mL, 6.13 mmol; 1 g/10 mL) with the subsequent formation of a precipitate. Each complex was purified by flash chromatography on silica gel using a gradient of DCM in acetone (0–10%). The purified complex was redissolved in a minimum amount of MeOH and precipitated again by adding it to an aqueous NH_4PF_6 solution (10 mL; 1 g/10 mL). The title complex was filtered, washed with water and dried under vacuum.

Complex 1a [Ir (Fphtl)$_2$(PytlPh)]$^+$PF$_6^-$

The complex was recrystallized in dichloromethane–Et_2O. Yield: 70%. ^{1}H NMR (300 MHz, CD_3CN) δ (ppm): 9.16 (s, 1H), 8.21–8.05 (m, 4H), 8.02 (d, J = 5.5 Hz, 1H), 7.72–7.58 (m, 5H), 7.52 (ddd, J = 14.2, 8.4, 5.7 Hz, 2H), 7.43–7.31 (m, 7H), 7.26–7.16 (m, 4H), 6.82–6.63 (m, 2H), 5.88 (ddd, J = 10.3, 8.0, 2.6 Hz, 2H), 5.51–5.45 (m, 4H). ^{19}F{^{1}H} NMR (282 MHz, CD_3CN) δ (ppm): −72.94 (d, J = 706.3 Hz), −113.74 (s), −114.68 (s). HR-MS: calculated ($C_{43}H_{32}F_2IrN_{10}$): 919.2405; found: 919.2379. Elemental analysis: calculated ($C_{43}H_{32}F_8IrN_{10}P$): C: 48.54%; H: 3.03%; N: 13.16%; found: C: 48.31%; H: 3.07%; N: 13.17%.

Complex 1b [Ir (dFphtl)$_2$(PytlPh)]$^+$PF$_6^-$

Recrystallization in dichloromethane–Et_2O. Yield: 81%. ^{1}H NMR (300 MHz, CD_2Cl_2) δ (ppm): 9.19 (s, 1H), 8.38 (d, J = 7.9 Hz, 1H), 8.10 (td, J = 7.8, 1.5 Hz, 1H), 8.04 (d, J = 5.5 Hz, 1H), 7.86–7.78 (m, 2H), 7.75 (m, 2H), 7.65–7.49 (m, 3H), 7.46–7.20 (m, 11H), 6.71–6.40 (m, 2H), 5.76 (m, 2H), 5.49 (m, 4H). ^{19}F{^{1}H} NMR (282 MHz, CD_2Cl_2) δ (ppm): −72.49 (d, J = 711.1 Hz), −108.97 (d, J = 7.8 Hz), −109.90 (d, J = 7.4 Hz), −111.52 (d, J = 7.8 Hz), −112.37 (d, J = 7.4 Hz). HR-MS: calculated ($C_{43}H_{30}F_4IrN_{10}$): 955.2215; found: 955.2188. Elemental analysis: calculated ($C_{43}H_{30}F_{10}IrN_{10}P$): C: 46.95%; H: 2.75%; N: 12.73; found: C: 46.88%; H: 2.90%; N: 12.86%.

Complex 2a [Ir (Fphtl)$_2$(PytlBn)]$^+$PF$_6^-$

Purified *via* silica gel column chromatography (dichloromethane–acetone (9 : 1)) and precipitated as the PF_6 salt after dissolving in a minimum amount of MeOH and by adding a NH_4PF_6 (1 g/10 mL) aqueous solution. Beige solid. Yield: 25%. ^{1}H NMR (400 MHz, CD_3CN) δ (ppm): 8.64 (s, 1H), 8.12 (s, 1H), 8.10 (s, 1H), 8.06–8.03 (m, 2H), 8.01 (dt, J = 5.6, 1.3 Hz, 1H), 7.57–7.49 (m, 2H), 7.44–7.33 (m, 8H), 7.30–7.20 (m, 5H), 6.77 (ddd, J = 9.3, 8.4, 2.6 Hz, 1H), 6.70 (ddd, J = 9.2, 8.4, 2.6 Hz, 1H), 5.88 (t, J = 2.4 Hz, 1H), 5.86 (t, J = 2.4 Hz, 1H), 5.71–5.59 (m, 3H), 5.50 (s, 6H). ^{19}F NMR {^{1}H} (282 MHz, CD_3CN) δ (ppm): −72.94 (d, J = 706.3 Hz), −113.77 (s), −114.70 (s). HR-MS: calculated ($C_{44}H_{34}F_2IrN_{10}$): 933.2568; found: 933.2598. Elemental analysis: calculated ($C_{44}H_{34}F_8IrN_{10}P$): C: 49.02%; H: 3.18%; N: 12.99; found: C: 49.17%; H: 3.19%; N: 12.00%.

Complex 2b [Ir (dFphtl)$_2$(PytlBn)]$^+$PF$_6^-$

Purified *via* silica gel column chromatography (dichloromethane–acetone (9 : 1)) and precipitated as the PF_6 salt after dissolving in a minimum amount of MeOH and by adding a NH_4PF_6 (1 g/10 mL) aqueous solution. White solid. Yield: 31%. ^{1}H NMR (300 MHz, DMSO) δ (ppm): 9.30 (s, 1H), 8.81 (dd, J = 3.1, 1.3 Hz, 2H), 8.35 (d, J = 7.7 Hz, 1H), 8.19 (td, J = 7.8, 1.5 Hz, 1H), 7.90 (d, J = 5.1 Hz, 1H), 7.58–7.49 (m, 1H), 7.42–7.28 (m, 9H), 7.25–7.11 (m, 6H), 6.94 (td, J = 10.0, 2.2 Hz, 1H), 6.84 (td, J = 10.0, 2.2 Hz, 1H), 5.90–5.73 (m, 2H), 5.70–5.62 (m, 4H), 5.60–5.51 (m, 2H). ^{19}F{^{1}H} NMR (282 MHz, DMSO) δ (ppm): −70.13 (d, J = 711.3 Hz), −108.87 (d, J = 7.4 Hz), −110.00 (d, J = 7.1 Hz), −110.85 (d, J = 7.5 Hz), −111.82 (d, J = 7.0 Hz). HR-MS: calculated ($C_{44}H_{32}F_4IrN_{10}$): 969.2380; found: 969.2385. Elemental analysis: calculated ($C_{44}H_{32}F_{10}IrN_{10}P$): C: 47.44%; H: 2.90%; N: 12.57; found: C: 47.02%; H: 2.87%; N: 12.00%.

Photophysical measurements

Absorption spectra were measured on a Varian Cary 5000 double-beam UV-vis-NIR spectrometer and are baseline corrected. Steady-state emission in the solid state was recorded on a HORIBA Jobin-Yvon IBH FL-322 Fluorolog 3 spectrometer equipped with a 450 W xenon-arc lamp, double-grating excitation and emission monochromators (2.1 nm mm^{-1} dispersion, 1200 grooves per mm), and a Hamamatsu R928 photomultiplier tube, while the steady-state emission spectra in the solution state were recorded on an Edinburgh FS920 spectrometer equipped with a 450 W xenon-arc lamp, excitation and emission monochromators (1.8 nm mm^{-1} dispersion, 1800 grooves per mm blazed at 500 nm), and a Hamamatsu R928 photomultiplier tube. Emission and excitation spectra were corrected for source intensity (lamp and grating) by standard correction curves. Time-resolved emission measurements were recorded in an Edinburgh Life Spec II spectrofluorimeter for solution and the HORIBA Jobin-Yvon IBH FL-322 Fluorolog 3 spectrometer for the solid state. The excitation wavelength was 375 nm or

295 nm, respectively, using a diode laser (FWHM 62 ps) and the time-correlated single photon counting (TCSPC) option was used for decay times. The quality of the fit was assessed by minimizing the reduced χ^2 function and by visual inspection of the weighted residuals. Deaerated samples were prepared by the freeze–pump–thaw technique. The photoluminescence quantum yields in MeCN were calculated using the relative method and quinine sulfate ($\Phi = 54\%$) in 0.5 N H_2SO_4 as the external standard.[11] Luminescence quantum yields in the solid state and thin films were measured with a Hamamatsu Photonics absolute PL quantum yield measurement system (C9920-02) equipped with a L9799-01 CW xenon light source (150 W), monochromator, C7473 photonic multichannel analyzer, and integrating sphere and employing U6039-05 PLQY measurement software (Hamamatsu Photonics, Ltd, Shizuoka, Japan).

Computations

Density Functional Theory (DFT) calculations. All calculations were performed with the Gaussian 09 (ref. 12) suite. The level of theory for all DFT[13] and TD-DFT[14] calculations was B3LYP; excited-state triplet geometries were calculated using the unrestricted B3LYP method (UB3LYP).[15] The 6-31G* basis set[16] was used for C, H and N directly linked to iridium while the other C, H, N and F atoms were undertaken with the 3-21G* basis set,[17] and the VDZ (valence double ζ) with the SBKJC effective core potential basis set[17a,18] was used for iridium. The predicted phosphorescence wavelengths were obtained by energy difference between the triplet and singlet states at their respective optimized geometries.[19] The energy, oscillator strength and related MO contributions for the 100 lowest singlet–singlet and 5 lowest singlet–triplet excitations were obtained from the TD-DFT/singlet and the TD-DFT/triplet output files, respectively. The calculated absorption spectra were visualized with GaussSum 2.1 (fwhm: 1000 cm^{-1}).[20]

Electrochemistry

The electrochemical characterization (cyclic voltammetry – CV and differential pulse voltammetry – DPV) for **1a**, **1b**, **2a** and **2b** was performed in acetonitrile (freshly distilled over CaH_2) with 0.1 M *n*-tetrabutylammonium hexafluorophosphate ($TBAPF_6$) added as the supporting electrolyte (electrochemical grade, 99%, Fluka). The concentration of the samples was 1 mM. Glassy carbon (CH Instrument vitreous carbon; $\varnothing = 3$ mm) was employed as the working electrode and was polished with 1 μm diamond paste before each recording. A platinum wire was used as the counter electrode, and a silver wire as a quasi-reference electrode (Ag-QRE), which was separated from the catholyte by a glass frit (Vycor). The reference electrode was calibrated at the end of each experiment against the ferrocene/ferricenium couple (Fc/Fc^+), whose formal potential is 0.4 V,[21] and data are reported against the KCl saturated calomel electrode (SCE). For the electrochemical experiments, a CHI750C electrochemical workstation (CH Instruments, Inc., Austin, TX) was used. The electrochemical experiments were performed in a glass cell under an argon atmosphere. An ohmic drop compensation was performed before each recording.

Device fabrication

Indium tin oxide (ITO) substrates (Thin Film Devices) were first cleaned by hand scrubbing with a non-ionic soap and water and then further cleaned in an ultrasonic water bath. Subsequently, the substrates went through UV ozone cleaning for 10 minutes. PEDOT:PSS (Clevios AI 4083) solutions were filtered through a 0.45 μm filter and then spin coated onto ITO substrates to reach the target thickness of 90 to 100 nm. The PEDOT:PSS films were baked at 100 °C for 10 minutes to remove water. Samples were then transferred into a nitrogen glove box with O_2 and H_2O levels lower than 1 ppm for the remaining steps. All four complexes were dissolved in acetonitrile at a concentration of 24 mg mL^{-1} and passed through a 0.1 μm filter. These solutions were spin coated onto the PEDOT:PSS covered ITO substrates, yielding active layer thicknesses of around 100 nm. Following this, the samples were baked at 120 °C for 60 min to remove the solvent. Samples were transferred into a thermal evaporator to deposit 1 nm of LiF and 80 nm of Al through a shadow mask to define twelve devices each with a 3 mm^2 area. A 760D electrochemical analyzer from CH Instruments (Austin, TX) was used for electrical testing. Radiant flux measurements were obtained with a calibrated Labsphere integrating sphere and photodiode, with photocurrents measured with a Keithley 6485 Picoammeter. An Ocean Optics Jazz spectrometer was used to measure the electroluminescence.

Results and discussion

Ligand and complex synthesis

The ligands 1-benzyl-4-(4-fluorophenyl)-1*H*-1,2,3-triazole (Fphtl), 1-benzyl-4-(2,4-difluorophenyl)-1*H*-1,2,3-triazole (dFphtl) and 2-(1-benzyl-1*H*-1,2,3-triazol-4-yl)pyridine (pytlBn) were obtained using our one-pot "Click" chemistry protocol[8] while 2-(1-phenyl-1*H*-1,2,3-triazol-4-yl)pyridine (pytlPh) was synthesized using PhN_3 and 2-trimethylsilylethynylpyridine under standard Click conditions.[22] The iridium dimers $[Ir(Fphtl)_2Cl]_2$ and $[Ir(dFphtl)_2Cl]_2$ were synthesized with sufficient thermal energy so as to produce exclusively the *trans* isomer with respect to the coordinating nitrogen atoms.[6a] The reaction of these iridium(III) dimers and the corresponding ancillary pyridyl triazole ligands in a mixture of $2\text{-}EtOCH_2CH_2OH$ and water (3 : 1) at 150 °C followed by anion metathesis with NH_4PF_6 yielded the desired complexes **1a–2b** as their hexafluorophosphate salts in good yields. All complexes were characterized by ^1H, $^{19}F\{^1H\}$, LR- and HR-MS and elemental analysis.

Electrochemical characterization

Cyclic voltammetry (CV) and differential pulse voltammetry (DPV) were used to investigate the electrochemical behavior and to assess the redox gap of these iridium complexes (see the ESI for CV traces, Fig. S1 and S2†). The electrochemical data are given *vs.* SCE and listed in Table 1. During the anodic scan all complexes undergo quasi-reversible oxidation processes

Table 1 Electrochemical data[a] of **1a**, **1b**, **2a** and **2b**. All potentials are given *vs.* SCE

Compound	$E_{1/2}^{Ox}$ (V)	ΔE_p[b] (V)	$E_{1/2}^{Red}$ (V)	ΔE_p[b] (V)	E_{HOMO}[c] (eV)	E_{LUMO}[c] (eV)	$\Delta E_{HOMO-LUMO}$ (eV)
1a	1.47[d] (1.51)	0.097	—(−1.76[e])	—	−5.67	−2.76	2.91
1b	1.63[d] (1.67)	0.084	—(−1.72[e])	—	−5.81	−2.79	3.01
2a	1.45[d] (1.51)	0.112	—1.81(−1.86[e])	0.096	−5.68	−2.73	2.95
2b	1.62[d] (1.67)	0.093	—1.78(−1.83[e])	0.099	−5.83	−2.74	3.09

[a] 1 mM of each complex in a mixture of CH_3CN and 0.1 M $TBAPF_6$, 298 K, glassy carbon 3 mm as the working electrode, $\nu = 0.1$ V s^{-1}. All potentials are given *vs.* SCE using the Fc/Fc^+ red–ox couple as an internal standard (0.40 V).[21] [b] ΔE_p was measured at 0.2 V s^{-1}, $\Delta E_p = |E_{pa} - E_{pc}|$. [c] The HOMO and LUMO energies were calculated using the relationship $E_{HOMO-LUMO} = -(E_{onset\ Ox./Red\ vs.\ Fc} + 4.8)$ eV.[23] [d] E_{pa}: anodic potential. [e] E_{pc}: cathodic potential.

ranging from 1.45 to 1.63 V. Upon cathodic sweep these complexes show irreversible (**1a** and **1b**) or quasi-irreversible behaviors (**2a** and **2b**) with the reduction potential falling within the range of −1.86 to −1.72 V.

On the basis of the onset potentials of the oxidation and reduction, the HOMO and LUMO energy levels were calculated relative to the energy levels of ferrocene (4.8 eV under vacuum).[23] As observed for cyclometallated Ir(III) complexes with 1-subtituted-4-aryl-1,2,3-1*H*-triazole as C^N ligands, the reduction is generally considered to occur on the N^N heterocycle of the ancillary ligand[6a,b] (in our case on the pyridine of the pyridyl triazole), whereas the oxidation processes largely involve the Ir atom, extending to the aryl ring of the aryltriazole.[6a,b,22,24]

The complexes **1b** and **2b** (1.63 and 1.62 V) containing dFphtl ligands show oxidation potentials higher than those functionalized with Fphtl, **1a** and **2a** (1.47 and 1.45 V). These potential shifts of 0.16 and 0.17 V, respectively, are in perfect agreement with the electron-withdrawing character of fluorine atoms observed for metallic complexes.[25] Complexes **1a** and **2a** or **1b** and **2b** have almost equal HOMO energy levels suggesting that the *N*-alkylation on the ancillary ligand does not play a significant role in the oxidation processes. However, this functionalization on the ancillary ligand is reflected in the reduction processes. Complexes **1a** and **1b**, incorporating a pytlPh N^N ligand that possesses extended conjugation, show irreversible behavior and a reoxidation process at *ca.* −0.8 V (see Fig. S1†). Complexes **2a** and **2b**, containing an *N*-benzyl group attached to the triazole (pytlBn) that breaks the aforementioned conjugation, exhibit more reversible CV behavior. The cathodic potentials (E_{pc}) are affected by the extended π conjugation over the phenyl substitution of the ancillary ligand by a less negative shift from −1.86 or −1.83 V (**2a** and **2b**) to −1.76 or −1.72 V (**1a** and **1b**), respectively. As expected, the reduction processes are only slightly perturbed by the fluorine substitution on the cyclometallated ligand.

The HOMO–LUMO energy gap ($\Delta E_{HOMO-LUMO}$) increases going from the Fphtl- to the dFphtl-based complexes. For **1a** and **1b**, the $\Delta E_{HOMO-LUMO}$ is 2.91 (426 nm) and 3.01 eV (412 nm) respectively. A similar trend is observed comparing **2a** and **2b**, for which the $\Delta E_{HOMO-LUMO}$ increases from 2.95 (421 nm) to 3.09 eV (407 nm), in agreement with the increased electron withdrawing ability of the cyclometallated ligands. However, changing the ancillary ligand, from a *N*-phenyl to a *N*-benzyl substituted pyridyl triazole has only a modest effect on the energy gap between the HOMO and the LUMO orbitals for **1a**/**2a** (0.04 eV) or **1b**/**2b** (0.08 eV).

Photophysical characterization

The 298 K absorption and emission spectra in acetonitrile, ACN, solution are shown in Fig. 1a while the emission spectra at 77 K in a 2-MeTHF glass are shown in Fig. 1b. The photophysical

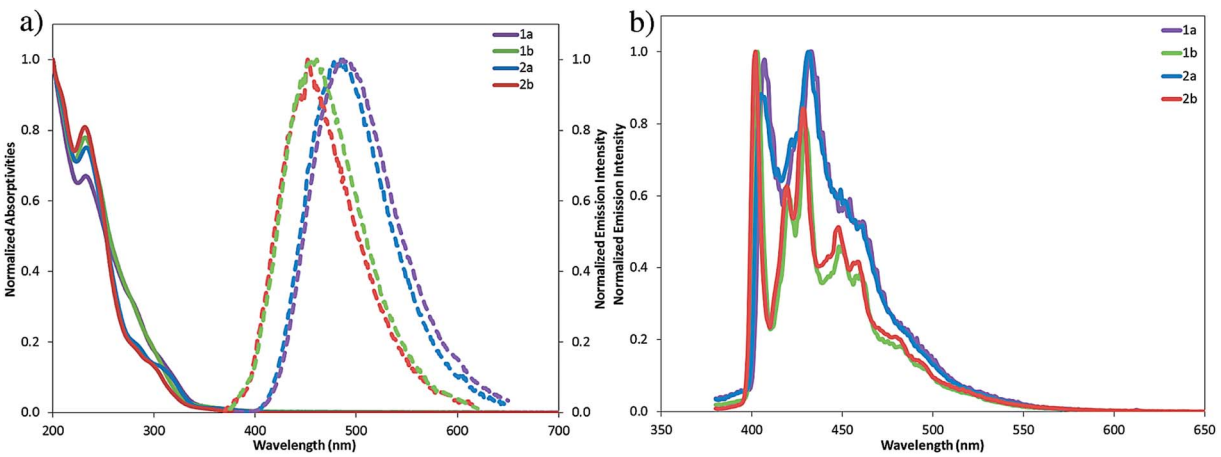

Fig. 1 (a) Absorption spectra (solid lines) and deaerated emission spectra (dashed lines) of complex **1a–2b**, in ACN at 298 K; (b) emission spectra of complexes **1a–2b**, in 2-MeTHF at 77 K. $\lambda_{exc} = 300$ nm.

Table 2 Photophysical data in acetonitrile solutions of the investigated complexes

Complex	Absorbance 298 K (nm) [Molar absorptivities] ($\times 10^4$ M^{-1} cm^{-1})	Emission 77 K[a] (nm)	298 K (nm)	Φ_{PL} N_2[a] (%)	τ_e 77 K[b,c] (μs)	298 K[b,c] (ns)
1a	233 [6.71]; 274 [3.17]; 300 [1.59]; 355 [0.12]	407 [0.98]; 433 [1.00]	487	0.3	3.90	5.5 (76.9%) 0.92 (23.1%)
1b	233 [6.90]; 296 [1.73]; 347 [1.31]	403 [1.00]; 429 [0.79]	461	0.03	7.50	1.6 (19.4%) 0.6 (77.4%) 7.6 (3.2%)
2a	232 [6.11]; 280 [1.71]; 300 [1.14]; 355 [0.10]	407 [0.87]; 431 [1.00]	485	0.2	4.42	62.3 (2.5%) 2.1 (52.9%) 5.1 (44.6%)
2b	233 [6.59]; 280 [1.61]; 295 [1.23]; 344 [0.13]	402 [1.00]; 428 [0.84]	452	0.05	6.72	10.4 (5.2%) 2.9 (22.5%) 0.5 (72.4%)

[a] Measured at 298 K using quinine sulfate ($\Phi = 54\%$) in 0.5 N H_2SO_4 as the external standard.[11] [b] Measured in the 2-MeTHF glass state at 77 K, and in ACN solution at room temperature (relative intensities). [c] $\lambda_{exc} = 375$ nm.

properties are summarized in Table 2. Analogous to other aryltriazole complexes, the strong absorption bands at about 235 nm (ε *ca.* 6.55×10^4 M^{-1} cm^{-1}) were assigned to strongly allowed $^1\pi$–π^* ligand-centered (^{1}LC) transitions.[6a,b,22] Additionally, the absorption spectra for each of the four complexes showed low intensity bands at around 300 nm (ε *ca.* 1.40×10^4 M^{-1} cm^{-1}). From the TD-DFT computations (*vide infra*), these bands are mixed ^{1}LC/^{1}MLCT transitions with contributions from both the C^N and N^N ligands. The transitions responsible for the low intensity shoulder that tapers off at around 400 nm are mixed ^{1}LLCT/^{1}MLCT transitions. In the tail of the band, at lower energy, ^{3}MLCT transitions are present. Generally, the profile of the absorption spectra differs slightly between complexes possessing a pytlPh (**1a** and **1b**) that are more highly absorptive between 270 and 300 nm and complexes bearing a pytlBn ligand (**2a** and **2b**).

In ACN solution at 298 K, the four complexes show unstructured deep blue to sky blue emission, with λ_{max} values ranging from 452 to 487 nm (Fig. 1a). The profile of these spectra suggests that each of the complexes is emitting from a mixed CT state.

The addition of increasing numbers of fluorine atoms, *i.e.* going from Fphtl to dFphtl, results in the expected higher energy emission. Thus, the emission of **1b** is blue-shifted by 1158 cm^{-1} (26 nm) compared to **1a**, while that of **2b** is blue-shifted by 1505 cm^{-1} (33 nm) compared to **2a**. This effect has been well described in many related systems and results from larger stabilization of the HOMO compared to the LUMO as a consequence of the electron withdrawing groups.[6b,7] By contrast, *N*-substitution of the pyridyl triazole ligand (Ph *vs.* Bn) does not appreciably affect the emission of the complexes as shown by smaller blue-shifts in the emission spectra between **1a** and **2a** (85 cm^{-1}) and between **1b** and **2b** (432 cm^{-1}). Thus, decreasing the conjugation length of the ancillary ligand in this particular manner does not significantly impact the overall emission energy. Previous work by De Cola and co-workers[7,26] on related pyridyl triazole systems and by Duan and Qiu *et al.*[27] on pyridyl pyrazole-containing cationic iridium complexes demonstrated that negligible electronic coupling was induced through different N-substitutions on the five-membered heterocycle. Compared to $[Ir(dFphtl)_2(bpy)]PF_6$ ($\lambda_{em} = 514$ nm in ACN), the emission maxima for complexes **1b** and **2b** are blue-shifted by 2237 cm^{-1} (53 nm) and 2669 cm^{-1} (62 nm), respectively, demonstrating the important color tuning capacity of the triazole ring.[6b] Indeed, this change in the emission can be attributed mainly to a higher lying LUMO of the pytl ligands compared to bpy.[7] In fact, to the best of our knowledge, among all the triazole-containing cationic iridium complexes reported to date, **1b** and **2b** are the bluest emitters in terms of both their emission maxima and the overall color purity.[6b,7,22,26,28]

The emission at 77 K in 2-MeTHF glass was also investigated (Fig. 1b). The emission spectra are highly structured and blue-shifted compared to those at 298 K, in agreement with the predominant CT character of the excited states.[29] Similar to the trends observed at 298 K, the same emission spectral profile exists for **1b** and **2b**, which emit at energies slightly higher compared to the spectra of **1a** and **2a**.

Photoluminescence quantum efficiencies (Φ_{PL}) were determined in ACN solutions using quinine sulfate as the external reference ($\Phi_{PL} = 54\%$).[11] Unfortunately, as with many blue emitters, **1a–2b** are very poorly luminescent with Φ_{PL} lower than 1%. The explanation for such low values will be discussed in the following section.

Time-resolved emission spectroscopy was used to quantify the excited state lifetimes (τ_e). Each of the complexes shows multi-exponential decay kinetics at 298 K in ACN. Excited state lifetimes were found to be extremely short for phosphors. Upon cooling to 77 K, τ_es were significantly longer, in the μs regime, and became monoexponential. Thompson *et al.*[30] elegantly showed that the excited state properties of *fac*-Ir(ppz)$_3$ (ppz = 1-phenylpyrazolyl) were strongly dependent on temperature due to the thermal population of non-radiative states. Complexes

Table 3 Photophysical data in the solid state

Complex	Sample	λ_{max} (nm)	Φ^a (%)	τ_e (ns)
1a	Powder	464	<1	3 (21%); 43 (34%); 484 (45%)
	Neat[b]	473	1	66 (8%); 340 (37%); 1138 (55%)
	50% in PMMA	461	2	64 (20%); 274 (49%); 895 (51%)
	10% in PMMA	452	3	54 (43%); 402 (57%)
1b	Powder	456	<1	4 (20%); 36 (29%); 370 (51%)
	Neat[b]	451	2	80 (20%); 665 (80%)
	50% in PMMA	437	<1	18 (12%); 96 (40%); 537 (47%)
	10% in PMMA	433	<1	10 (35%); 105 (64%)
2a	Powder	453	12	133 (21%); 330 (78%)
	Neat[b]	468	1	31 (12%); 152 (40%); 643 (47%)
	50% in PMMA	459	2	32 (9%); 158 (38%); 677 (54%)
	10% in PMMA	449	3	60 (8%); 296 (36%); 1100 (56%)
2b	Powder	435	10	200 (42%); 560 (57%)
	Neat[b]	454	2	58 (44%); 470 (55%)
	50% in PMMA	436	<1	48 (20%); 259 (45%)
	10% in PMMA	430	<1	100 (24%); 837 (76%)

[a] Measured using an integrating sphere. [b] Neat thin film.

1a–2b exhibit similar photophysical behaviour to *fac*-Ir(ppz)$_3$ in that they are also blue emitters with low Φ_{PL}, have short τ_e at 298 K and much longer τ_e at 77 K. Thus, by analogy we believe that access to non-radiative states should be responsible for the rapid quenching of the excited states in **1a–2b**.

As a prelude to incorporation of these complexes into matrices for devices, the solid state luminescence properties, both in powder and in thin films, were investigated. These measurements are summarized in Table 3 and the corresponding emission spectra can be found in the ESI (see Fig. S7–S11†). The emission spectra were first directly measured on powder samples. Thin films were obtained by spin-coating from ACN solutions of either the pristine complex or mixtures with differing amounts of PMMA. In all cases, the emission maximum was blue-shifted compared to the solution state. The Φ_{PL} values were determined with the aid of an integrating sphere. Notably, though Φ_{PL} values remained low for all **1a** and **1b** (*ca.* 1%), the Φ_{PL} of powder samples of **2a** and **2b** were enhanced at 10–12%. The increased Φ_{PL} is probably due to improved intermolecular spacing of luminophores conferred by the bulkier *N*-benzyl group compared to the *N*-phenyl moiety. The excited state decay kinetics in the solid state showed complex behaviour. In all cases, bi-exponential or even tri-exponential decays were observed, which could be rationalized due to the heterogeneity of the samples.

Computations

In order to better understand the origin of the opto-electronic properties of the complexes, a combined density functional theory (DFT) and time-dependent DFT (TDDFT) study was undertaken.[13c,14,31] All complexes were modeled using Gaussian

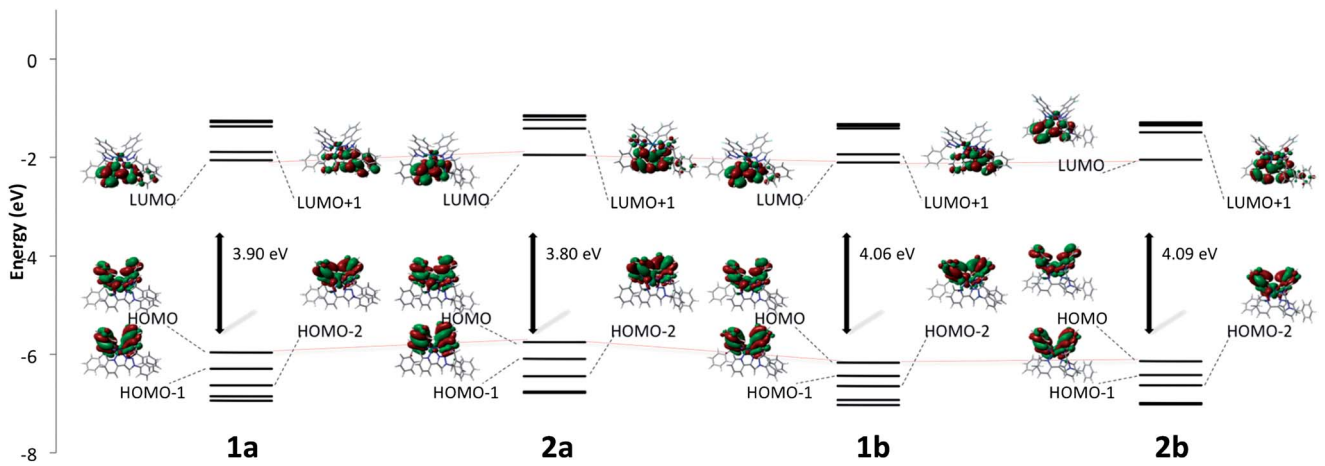

Fig. 2 Calculated energy level scheme for the Kohn–Sham orbitals between HOMO−5 to LUMO+5 of **1a**, and **2a** containing Fphtl cyclometallating ligands and **1b**, and **2b** containing dFphtl cyclometallating ligands, including contour plots of selected most relevant MOs and the associated DFT calculated HOMO–LUMO energy gap (in eV).

09[32] using the following DFT protocol at the B3LYP[15b,15c,33] level of theory with the SBKJC-DVZ[17a,18] basis set for iridium, 6-31G* for heavy atoms directly coordinated to iridium and 3-21G* for all other atoms.[17,34] An ACN quantum mechanical continuum solvation model was employed throughout the computational study.[35] We have previously shown that a similar computational methodology incorporating the SBKJC-DVZ basis set on iridium accurately predicts both ground and excited state properties for triazole-containing iridium complexes.[6b]

Each of the complexes adopts a pseudo-octahedral geometry. For the ground state optimized structures, increasing the fluorine-content on the C^N ligand results in a *ca.* 0.01 Å shortening of each of the Ir–C and Ir–N bonds while modification of the *N*-alkyl group did not affect the coordination sphere around the iridium atom. The geometry in the triplet state is essentially unchanged compared to that in the ground state. Globally, there is only a modest contraction of the Ir–N_{py} of the N^N ligand of *ca.* 0.05 Å in each of **1a–2b** and a small contraction of the Ir–C bond of *ca.* 0.04 Å for the Fphtl containing complexes (**1a** and **2a**).

Fig. 2 shows compiled Kohn–Sham energy diagrams of the five highest energy occupied and five lowest energy unoccupied molecular orbitals (MOs) for **1a–2b** along with contour plots of selected MOs. For each of the complexes, the HOMO is situated on both the C^N ligands and the metal center, accounting for, respectively, *ca.* 64% and 33% of the electron density distribution (*cf.* Fig. S12–S15† for quantification of the electron density distributions). The electron density distribution on the C^N ligands extends over both the aryl and triazole rings but the *N*-benzyl groups are themselves bereft of electron density. The HOMO−1 and HOMO−2 MOs for each of the complexes possess similar topologies, however the metal contribution

Table 4 Principal theoretical low energy singlet–singlet and singlet–triplet electronic transitions with corresponding oscillator strengths (*f*) and assignments for **1a**, **2a**, **1b**, and **2b**[a]

Complex	State	Nature of transition (contribution in %)	Primary character	Energy (eV)	Energy (nm)	Oscillator strength (*f*)
1a	S_1	HOMO → LUMO (78%), HOMO → L+1 (19%)	LLCT/MLCT	3.25	382	0.0004
	S_3	H−1 → LUMO (90%)	LLCT/MLCT	3.69	336	0.0124
	S_4	H−1 → L+1 (88%)	LLCT/MLCT	3.84	323	0.0159
	T_1	HOMO → LUMO (69%), HOMO → L+1 (24%) H−1 → L+4 (11%), H−1 → +6 (14%), HOMO → L+3 (16%),	LLCT/MLCT	3.22	385	0.0000
	T_2	HOMO → L+4 (11%), HOMO → L+5 (16%) H−1 → L+3 (11%), H−1 → L+5 (19%), HOMO → L+4 (12%),	LC_{Fphtl}	3.33	373	0.0000
	T_3	HOMO → L+6 (17%)	LC_{Fphtl}	3.35	370	0.0000
2a	S_1	HOMO → LUMO (97%)	LLCT/MLCT	3.15	394	0.0008
	S_9	H−5 → LUMO (29%), H−4 → LUMO (19%), H−3 → LUMO (44%)	LLCT/MLCT	4.14	300	0.1351
	S_{11}	HOMO → L+5 (87%)	LC_{Fphtl}	4.22	294	0.1802
	T_1	HOMO → LUMO (94%) H−1 → L+4 (11%), H−1 → L+6 (12%), HOMO → L+3 (28%),	LLCT/MLCT	3.12	397	0.0000
	T_2	HOMO → L+5 (18%) H−1 → L+3 (14%), H−1 → L+5 (17%), HOMO → L+4 (24%),	LC_{Fphtl}	3.30	376	0.0000
	T_3	HOMO → L+6 (16%)	LC_{Fphtl}	3.33	372	0.0000
1b	S_1	HOMO → LUMO (80%), HOMO → L+1 (17%)	LLCT/MLCT	3.39	366	0.0002
	S_3	H−1 → LUMO (91%)	LLCT/MLCT	3.77	329	0.0171
	S_5	H−2 → LUMO (48%), H−1 → L+1 (30%)	LLCT/MLCT	3.95	314	0.0287
	T_1	HOMO → LUMO (39%), HOMO → L+1 (16%)	LLCT/MLCT	3.34	371	0.0000
	T_2	H−3 → LUMO (16%), HOMO → L+3 (17%) H−1 → L+3 (16%), H−1 → L+5 (11%), HOMO → L+2 (24%),	LLCT/MLCT/LC_{pytlph}	3.38	367	0.0000
	T_3	HOMO → L+6 (13%)	LC_{dFphtl}/MLCT	3.39	366	0.0000
2b	S_1	HOMO → LUMO (96%)	LLCT/MLCT	3.41	363	0.0010
	S_2	H−1 → LUMO (98%)	LLCT/MLCT	3.83	324	0.0117
	T_1	HOMO → LUMO (59%) H−1>L+3 (10%), H−1 → L+6 (13%), HOMO → L+2 (24%),	LLCT/MLCT	3.36	369	0.0000
	T_2	HOMO → L+5 (11%) H−1 → L+2 (14%), H−1 → L+5 (16%), HOMO → L+3 (16%),	LC_{dFphtl}/LLCT	3.38	366	0.0000
	T_3	HOMO → L+6 (16%)	LC_{dFphtl}/LLCT	3.40	364	0.0000

[a] H = HOMO; L = LUMO; MLCT = metal-to ligand charge transfer; LLCT = ligand to-ligand charge transfer; LC = ligand-centered.

decreases significantly to *ca.* 4% and 20%, respectively, for these two MOs. The LUMO for each of the four complexes is situated exclusively (electron density distribution *ca.* 96%) on the pyridyl triazole ligand. The LUMO+1 and LUMO+2 are also predominantly on the pyridyl triazole. However, there are two major differences between the *N*-phenyl and the *N*-benzyl substituted complexes (**1a** and **1b** *vs.* **2a** and **2b**): (i) the LUMO+1 contains an important contribution from the conjugated phenyl group in **1a** and **1b** while in **2a** and **2b** such a contribution is impossible due to the lack of conjugation between the tl and the Bn group; (ii) secondly the LUMO+2 in **1b** and **2b** contains significant contributions from the cyclometallating ligands (41% for **2a** and 60% for **2b**).

The MOs for dFphtl-containing complexes **1b** and **2b** are stabilized compared to Fphtl-containing analogs **1a** and **2a**. The stabilization is more pronounced for the occupied MOs resulting in a 0.16–0.19 eV increase in the HOMO–LUMO gap with the incorporation of additional fluorine groups at the 2-position of the aryltriazole. The energies of the MOs are somewhat less perturbed by the nature of the *N*-alkyl group on the pyridyl triazole. Both the HOMO and LUMO are slightly stabilized for complexes containing an *N*-phenyl group (**1a** and **1b**) compared to those containing an *N*-benzyl group (**2a** and **2b**). Interestingly, the HOMO stabilization is more pronounced for the Fphtl-containing complexes, resulting in a net increase in the HOMO–LUMO gap for **1a** compared to **2a**, while the HOMOs for **1b** and **2b** are pseudo isoenergetic, resulting in a net decrease in the HOMO–LUMO gap of 0.03 eV. Generally, the picture provided by the DFT computations is consistent with the CV data presented in Table 1.

TDDFT calculations of the 100 lowest-energy vertical singlet–singlet and 5 lowest-energy singlet–triplet transitions were performed in order to permit assignment of the nature of the different absorption bands and to elucidate the nature of the emission. Comparisons between computed and experimental absorption spectra are reported in Fig. S16–S19.† The most important low energy vertical transitions are collated in Table 4. The nature of the low energy absorption bands (>300 nm) is best characterized as an admixture of metal-to-ligand and ligand-to-ligand charge transfer transitions. The intense absorption bands around 250 nm are a mixture of different ligand-centered (LC) transitions. The nature of the T_1 state can also be described as mixed CT. Notably, for each of the four complexes, the T_2 and T_3 states are very close in energy to the T_1, <0.21 eV for Fphtl complexes **1a** and **2a**, and <0.05 eV for dFphtl complexes **1b** and **2b**. These triplet states are largely $LC_{C\hat{}N}$ in nature.

The geometry and energy of the T_1 state for each complex were fully optimized using unrestricted B3LYP (UB3LYP). The spin densities for the T_1 state are shown in Fig. 3. For **1a** and **2a**, the spin density is distributed throughout the complex, residing on both the aryltriazole and pyridyl triazole ligands along with contributions from iridium while for **1b** and **2b** the spin density is localized to a greater extent on the pyridyl triazole ligand along with the metal. This would suggest that though emission for each of the four complexes can be best described as resulting from an admixture of ^{3}MLCT/^{3}LLCT, in agreement with the TD-DFT analysis, the nature of the emission in **1a** and **2a** points to an increased ligand-centered character with respect to the Fphtl ligand. The predicted emission energy as determined by the ΔSCF approach is 401, 420, 389 and 386 nm, respectively, for **1a**, **2a**, **1b**, and **2b**. These predictions compare very well to the $E_{0,0}$ band at 77 K, which are 407, 403, 407 and 402 nm, respectively, for **1a**, **1b**, **2a**, and **2b**. The substitution pattern of the complexes influences strongly the magnitude and orientation of the excited state dipoles (*cf.* Fig. S20–S23†). There is a large decrease in the magnitude of the dipole moment in the T_1 state compared to the S_0 state for **1a** and **1b** (5.6–9.3 D), complexes bearing the Fphtl C^N ligand. This effect is attenuated somewhat for the dFphtl analogs, with a more modest decrease of *ca.* 2.3 D calculated between the excited and ground states. For **1a–2b**, the ground state dipole is oriented as to bifurcate the ancillary ligand. This relative orientation is conserved in **1b** and **2b** in the triplet state.

Device characterization

Electroluminescent devices of layering Al/LiF/iTMC/PEDOT:PSS/ITO were tested at a constant voltage under a nitrogen

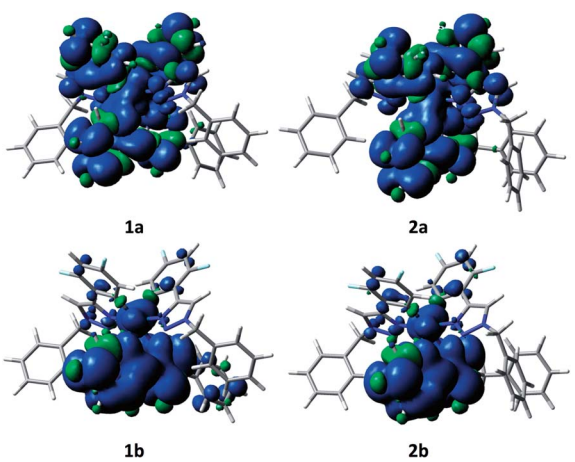

Fig. 3 Calculated spin density contours of the T_1 state for **1a**, **2a**, **1b** and **2b** (isocontour value of 0.0004 au).

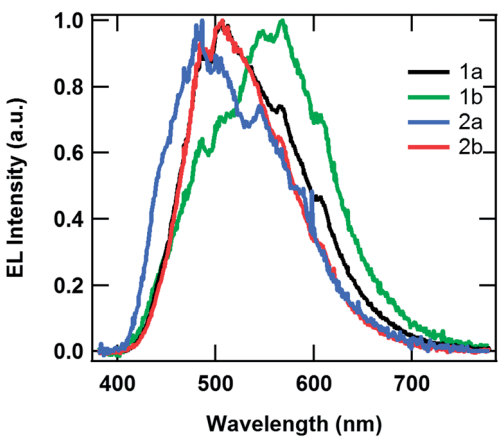

Fig. 4 Electroluminescence spectra of Al/LiF/iTMC/PEDOT:PSS/ITO devices under 9 V bias, where the iTMC is complex **1a–2b**.

atmosphere in a glovebox. All devices turned on with yellowish-green to blue emission with structured electroluminescence (EL) peaks, as in Fig. 4 for devices under a 9 V applied bias. Similar to the trends observed for emission in the bulk, **2a** and **2b** were more blue-shifted than **1a** and **1b**, which may result from the shorter conjugation length from the *N*-benzyl-substitution on the pyridyl triazole in both **2a** and **2b**. Luminophore **2a** is a deep blue emitter, with an EL spectral peak and CIE coordinates (0.26, 0.36) similar to the previously reported bluest iTMC emitters.[7,36]

The EL spectra were all red shifted compared with the solution or the thin film PL spectra. The EL spectra are significantly broader. This widening and red-shifting of the spectra is suggestive of excimer formation. Likewise, large red-shifting of EL spectra has been observed previously in fluoro-substituted Ir iTMC analogs and ascribed to the multiple triplet energy states available for emission, behaviour of which has also been predicted by computations for **1a** and **2a**.[37] Remarkably, in the devices the effect of fluorine atoms on blue-shifting is reversed relative to what is observed in solution or thin films with **1a** blue-shifted compared to **1b** and likewise **2a** blue-shifted compared to **2b**. This behavior could be due to the different surface properties of the film on an ionic polymer mixture *versus* directly on glass, or it may indicate greater instability and excimer formation under the high exciton concentrations associated with device driving.[38]

To understand this further, we explored the red-shifting of the EL by testing the devices at higher biases and recording the changes in spectra over time. Fig. 5 shows the evolution of the device emission over time at 14 V applied bias. The blue curve indicates the spectra taken just after device turn on, and the red curve is obtained approximately 10 minutes later. As for 9 V, all spectra are red-shifted when compared to their PL counterparts.

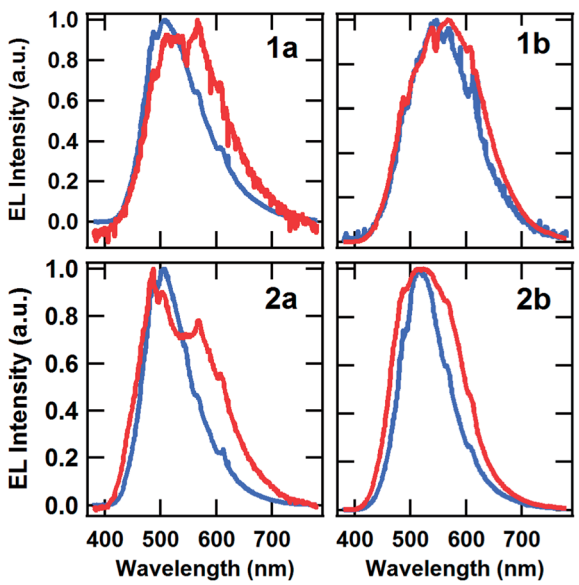

Fig. 5 Electroluminescence spectra of Al/LiF/iTMC/PEDOT:PSS/ITO devices under 14 V bias, where the iTMC is complex **1a–2b**. The blue curve indicates the first spectrum taken shortly after device turn on, while the red curve is a spectrum recorded 10 min later.

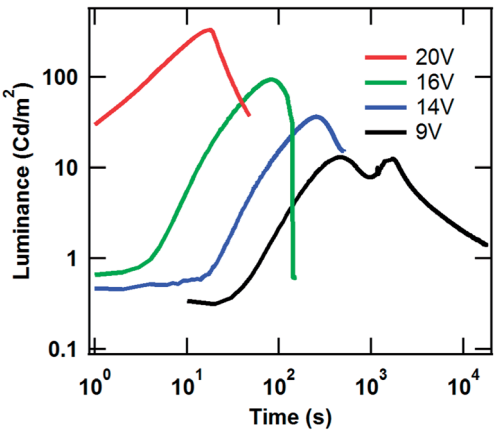

Fig. 6 Luminance *versus* time for Al/LiF/**2a**/PEDOT:PSS/ITO electroluminescent devices operated under various constant voltages.

Furthermore, in all four cases the spectra broaden and red-shift with time, consistent with the formation of excimers.[38]

Fig. 6 shows the effect of driving a Al/LiF/**2a**/PEDOT:PSS/ITO device under various constant voltages while Fig. 7 displays an image of the operational LEEC. At 20 V, the device reaches a maximum luminance of over 300 cd m^{-2}, but is very short lived, with a half-life on the order of seconds. Lifetime is increased as voltage is reduced: for 9 V driving the lifetime is close to 1 h. However, the luminance maximum is also reduced as voltage is decreased, showing the trade-off between maximum luminance and lifetime.[2a] Table 5 shows the EL data for all four complexes. The external quantum efficiencies (EQE) for different complexes are all on the order of 0.1–0.5%, which correlates with low Φ_{PL} in thin films. The luminance values of the other complexes are

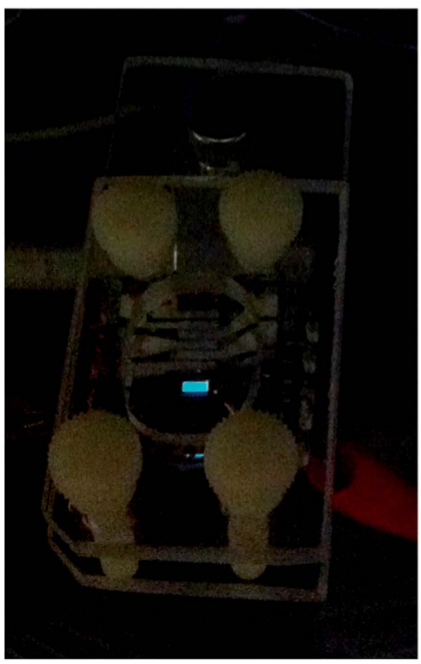

Fig. 7 LEEC of complex **2a**.

Table 5 Summary of electroluminescence and device data for 9 V operation

Complex	EL λ_{max} (nm)	EQE[a] (%)	Current efficiency (cd A^{-1})	Max. brightness (cd m^{-2})	Turn on time (h)	Lifetime $t_{1/2}$ (h)	CIE coordinates	
							x	y
1a	508	0.48	1.4	25	0.7	1.2	0.3065	0.4434
1b	569	0.45	1.3	7	1.5	6	0.3658	0.4504
2a	487	0.14	0.3	13	0.1	0.8	0.2640	0.3632
2b	508	0.39	0.4	3	2	6	0.2799	0.4494

[a] Estimated.

similar to that of **2a** at 9 V driving, on the order of ~10 cd m^{-2}, and the half-lives of the luminance were on the order of hours. The monofluoro compounds **1a** and **2a** showed higher luminance, faster turn on times and shorter half-lives than the difluoro analogs **1b** and **2b**.

Conclusions

Four cationic heteroleptic iridium complexes bearing fluorinated aryltriazole cyclometallating and pyridyltriazole ancillary ligands have been synthesized and their optoelectronic properties in both solution and the solid state extensively characterized. All four complexes are deep blue emitters both in solution and in the solid state but with very low quantum efficiencies and complex decay kinetics with short excited state lifetimes. The EL spectra of these complexes were all red-shifted in comparison to their PL spectra. Nonetheless, emitter **2a** is among the bluest devices reported to date (λ_{max} = 487 nm). External quantum efficiencies were limited by the low inherent quantum yield of the material, and device lifetimes were compromised by the high voltages required for ionic redistribution for efficient carrier injection. Our findings suggest that excimer formation limits device performance.

Acknowledgements

EZ-C acknowledges CFI (Canadian Foundation for Innovation), NSERC (the National Sciences and Engineering Research Council of Canada), FQRNT (Le Fonds québécois de la recherche sur la nature et les technologies) and the Université de Sherbrooke for financial support. SL acknowledges FQRNT for a doctoral scholarship and the Centre Québecois sur la matériaux fonctionnels (CQMF) for a travel scholarship to work in LDC's laboratory. JMF-H would like to acknowledge Fundación Séneca (Agencia Regional de Investigación, Región de Murcia) for a grant. The authors thank Dr Matteo Mauro for help with excited state lifetime measurements.

References

1 Q. Pei, G. Yu, C. Zhang, Y. Yang and A. J. Heeger, *Science*, 1995, **269**, 1086–1088.
2 (*a*) J. D. Slinker, J. Rivnay, J. S. Moskowitz, J. B. Parker, S. Bernhard, H. D. Abruña and G. G. Malliaras, *J. Mater. Chem.*, 2007, **17**, 2976–2988; (*b*) R. D. Costa, E. Ortí, H. J. Bolink, F. Monti, G. Accorsi and N. Armaroli, *Angew. Chem., Int. Ed.*, 2012, **51**, 8178–8211.
3 A. A. Gorodetsky, S. T. Parker, J. D. Slinker, D. A. Bernards, M. H. Wong, S. Flores-Torres, H. D. Abruña and G. G. Malliaras, *Appl. Phys. Lett.*, 2004, **84**, 807.
4 (*a*) D. A. Bernards, J. D. Slinker, G. G. Malliaras, S. Flores-Torres and H. D. Abruna, *Appl. Phys. Lett.*, 2004, **84**, 4980–4982; (*b*) J. D. Slinker, J. Rivnay, J. A. DeFranco, D. A. Bernards, A. A. Gorodetsky, S. T. Parker, M. P. Cox, R. Rohl, G. G. Malliaras, S. Flores-Torres and H. D. Abruña, *J. Appl. Phys.*, 2006, **99**, 074502.
5 T. Hu, L. He, L. Duan and Y. Qiu, *J. Mater. Chem.*, 2012, **22**, 4206–4215.
6 (*a*) J. M. Fernández-Hernández, C.-H. Yang, J. I. Beltrán, V. Lemaur, F. Polo, R. Frõhlich, J. Cornil and L. De Cola, *J. Am. Chem. Soc.*, 2011, **133**, 10543–10558; (*b*) S. Ladouceur, D. Fortin and E. Zysman-Colman, *Inorg. Chem.*, 2011, **50**, 11514–11526; (*c*) J. M. Fernández-Hernández, J. I. Beltrán, V. Lemaur, M.-D. Gálvez-López, C.-H. Chien, F. Polo, E. Orselli, R. Fröhlich, J. Cornil and L. De Cola, *Inorg. Chem.*, 2013, **52**, 1812–1824; (*d*) K. Hasan and E. Zysman-Colman, *Inorg. Chem.*, 2012, **51**, 12560–12564; (*e*) L. Donato, P. Abel and E. Zysman-Colman, *Dalton Trans.*, 2013, **42**, 8402–8412.
7 M. Mydlak, C. Bizzarri, D. Hartmann, W. Sarfert, G. Schmid and L. De Cola, *Adv. Funct. Mater.*, 2010, **20**, 1812–1820.
8 S. Ladouceur, A. M. Soliman and E. Zysman-Colman, *Synthesis*, 2011, **2011**(3604), 3611.
9 F. Friscourt and G.-J. Boons, *Synthesis*, 2011, **22**, 3604–3611.
10 M. Nonoyama, *Bull. Chem. Soc. Jpn.*, 1974, **47**, 767–768.
11 W. H. Melhuish, *J. Phys. Chem.*, 1961, **65**, 229–235.
12 M. J. Frisch, G. W. Trucks, H. B. Schlegel, G. E. Scuseria, M. A. Robb, J. R. Cheeseman, G. Scalmani, V. Barone, B. Mennucci, G. A. Petersson, H. Nakatsuji, M. Caricato, X. Li, H. P. Hratchian, A. F. Izmaylov, J. Bloino, G. Zheng, J. L. Sonnenberg, M. Hada, M. Ehara, K. Toyota, R. Fukuda, J. Hasegawa, M. Ishida, T. Nakajima, Y. Honda, O. Kitao, H. Nakai, T. Vreven, J. A. Montgomery, J. E. Peralta, F. Ogliaro, M. Bearpark, J. J. Heyd, E. Brothers, K. N. Kudin, V. N. Staroverov, R. Kobayashi, J. Normand, K. Raghavachari, A. Rendell, J. C. Burant, S. S. Iyengar, J. Tomasi, M. Cossi, N. Rega, J. M. Millam, M. Klene, J. E. Knox, J. B. Cross, V. Bakken, C. Adamo, J. Jaramillo, R. Gomperts, R. E. Stratmann, O. Yazyev, A. J. Austin, R. Cammi, C. Pomelli, J. W. Ochterski,

R. L. Martin, K. Morokuma, V. G. Zakrzewski, G. A. Voth, P. Salvador, J. J. Dannenberg, S. Dapprich, A. D. Daniels, Ö. Farkas, J. B. Foresman, J. V. Ortiz, J. Cioslowski and D. J. Fox, Gaussian Inc., Wallingford, CT, 2009.

13 (*a*) P. Hohenberg and W. Kohn, *Phys. Rev. B: Solid State*, 1964, **136**, 864; (*b*) W. Kohn and L. Sham, *Phys. Rev.*, 1965, **140**, 1133; (*c*) *The Challenge of d and f Electrons*, ed. D. R. Salahub and M. C. Zerner, ACS, Washington, DC, 1989; (*d*) R. G. Parr and W. Yang, *Density-functional theory of atoms and molecules*, Oxford Univ. Press, Oxford, 1989.

14 (*a*) R. E. Stratmann, G. E. Scuseria and M. J. Frisch, *J. Chem. Phys.*, 1998, **109**, 8218; (*b*) R. Bauernschmitt and R. Ahlrichs, *Chem. Phys. Lett.*, 1996, **256**, 454; (*c*) M. E. Casida, C. Jamorski, K. C. Casida and D. R. Salahub, *J. Chem. Phys.*, 1998, **108**, 4439.

15 (*a*) A. D. Becke, *J. Chem. Phys.*, 1993, **98**, 5648–5652; (*b*) C. Lee, W. Yang and R. G. Parr, *Phys. Rev. B: Condens. Matter Mater. Phys.*, 1988, **37**, 785–789; (*c*) B. Miehlich, A. Savin, H. Stoll and H. Preuss, *Chem. Phys. Lett.*, 1989, **157**, 200–206.

16 V. A. Rassolov, J. A. Pople, M. A. Ratner and T. L. Windus, *J. Chem. Phys.*, 1998, **109**, 1223–1229.

17 (*a*) J. S. Binkley, J. A. Pople and W. J. Hehre, *J. Am. Chem. Soc.*, 1980, **102**, 939; (*b*) M. S. Gordon, J. S. Binkley, J. A. Pople, W. J. Pietro and W. J. Hehre, *J. Am. Chem. Soc.*, 1982, **104**, 2797; (*c*) W. J. Pietro, M. M. Francl, W. J. Hehre, D. J. Defrees, J. A. Pople and J. S. Binkley, *J. Am. Chem. Soc.*, 1982, **104**, 5039; (*d*) K. D. Dobbs and W. J. Hehre, *J. Comput. Chem.*, 1986, **7**, 359; (*e*) K. D. Dobbs and W. J. Hehre, *J. Comput. Chem.*, 1987, **8**, 861; (*f*) K. D. Dobbs and W. J. Hehre, *J. Comput. Chem.*, 1987, **8**, 880.

18 (*a*) W. J. Stevens, W. J. Basch and M. Krauss, *J. Chem. Phys.*, 1984, **81**, 6026; (*b*) W. J. Stevens, M. Krauss, H. Basch and P. G. Jasien, *Can. J. Chem.*, 1992, **70**, 612; (*c*) T. R. Cundari and W. J. Stevens, *J. Chem. Phys.*, 1993, **98**, 5555–5565.

19 (*a*) S. Ladouceur, D. Fortin and E. Zysman-Colman, *Inorg. Chem.*, 2010, **49**, 5625–5641; (*b*) M. S. Lowry, W. R. Hudson, R. A. Pascal Jr and S. Bernhard, *J. Am. Chem. Soc.*, 2004, **126**, 14129–14135.

20 N. M. O'Boyle, *GaussSum 2.0*, Dublin City University, Dubin Ireland, 2006.

21 N. G. Connelly and W. E. Geiger, *Chem. Rev.*, 1996, **96**, 877–910.

22 M. Felici, P. Contreras-Carballada, Y. Vida, J. M. M. Smits, R. J. M. Nolte, L. De Cola, R. M. Williams and M. C. Feiters, *Chem.–Eur. J.*, 2009, **15**, 13124–13134.

23 C. M. Cardona, W. Li, A. E. Kaifer, D. Stockdale and G. C. Bazan, *Adv. Mater.*, 2011, **23**, 2367–2371.

24 (*a*) Y. You and S. Y. Park, *Dalton Trans.*, 2009, 1267–1282; (*b*) Y. Chi and P.-T. Chou, *Chem. Soc. Rev.*, 2010, **39**, 638–655.

25 (*a*) I. R. Laskar and T.-M. Chen, *Chem. Mater.*, 2003, **16**, 111–117; (*b*) P. Coppo, E. A. Plummer and L. De Cola, *Chem. Commun.*, 2004, 1774–1775.

26 M. Felici, P. Contreras-Carballada, J. M. M. Smits, R. J. M. Nolte, R. M. Williams, L. De Cola and M. C. Feiters, *Molecules*, 2010, **15**, 2039–2059.

27 L. He, D. Ma, L. Duan, Y. Wei, J. Qiao, D. Zhang, G. Dong, L. Wang and Y. Qiu, *Inorg. Chem.*, 2012, **51**, 4502–4510.

28 (*a*) S. Zanarini, M. Felici, G. Valenti, M. Marcaccio, L. Prodi, S. Bonacchi, P. Contreras-Carballada, R. M. Williams, M. C. Feiters, R. J. M. Nolte, L. De Cola and F. Paolucci, *Chem.–Eur. J.*, 2011, **17**, 4640–4647; (*b*) S. Liu, P. Müller, M. K. Takase and T. M. Swager, *Inorg. Chem.*, 2011, **50**, 7598–7609; (*c*) B. Beyer, C. Ulbricht, D. Escudero, C. Friebe, A. Winter, L. González and U. S. Schubert, *Organometallics*, 2009, **28**, 5478–5488; (*d*) M. Juríček, M. Felici, P. Contreras-Carballada, J. Lauko, S. Rodríguez Bou, P. H. J. Kouwer, A. M. Brouwer and A. E. Rowan, *J. Mater. Chem.*, 2011, **21**, 2104–2111; (*e*) M. Juríček, P. H. J. Kouwer and A. E. Rowan, *Chem. Commun.*, 2011, **47**, 8740–8749; (*f*) E. Orselli, R. Q. Albuquerque, P. M. Fransen, R. Frohlich, H. M. Janssen and L. De Cola, *J. Mater. Chem.*, 2008, **18**, 4579–4590; (*g*) K. N. Swanick, S. Ladouceur, E. Zysman-Colman and Z. Ding, *Chem. Commun.*, 2012, **48**, 3179–3181; (*h*) M. de Barros e Silva Botelho, J. M. Fernandez-Hernandez, T. B. de Queiroz, H. Eckert, L. De Cola and A. S. S. de Camargo, *J. Mater. Chem.*, 2011, **21**, 8829–8834; (*i*) D. Sykes and M. D. Ward, *Chem. Commun.*, 2011, **47**, 2279–2281.

29 R. D. Costa, F. Monti, G. Accorsi, A. Barbieri, H. J. Bolink, E. Ortí and N. Armaroli, *Inorg. Chem.*, 2011, **50**, 7229–7238.

30 T. Sajoto, P. I. Djurovich, A. B. Tamayo, J. Oxgaard, W. A. Goddard and M. E. Thompson, *J. Am. Chem. Soc.*, 2009, **131**, 9813–9822.

31 (*a*) P. Hohenberg and W. Kohn, *Phys. Rev. B: Solid State*, 1964, **136**, B864; (*b*) W. Kohn and L. J. Sham, *Phys. Rev.*, 1965, **140**, A1133.

32 M. J. Frisch, G. W. Trucks, H. B. Schlegel, G. E. Scuseria, M. A. Robb, J. R. Cheeseman, V. G. Zakrzewski, J. A. Montgomery, R. E. Stratmann, J. C. Burant, S. Dapprich, M. J. Millam, A. D. Daniels, K. N. Kudin, M. C. Strain, O. Farkas, J. Tomasi, V. Barone, M. Cossi, R. Cammi, B. Mennucci, C. Pomelli, C. Adamo, S. Clifford, J. Ochterski, G. A. Peterson, P. Y. Ayala, Q. Cui, K. Morokuma, A. Malik, A. D. Rabuck, K. Raghavachari, J. B. Foresman, J. Cioslowski, J. V. Ortiz, A. G. Baboul, B. B. Stefanov, G. Liu, A. Liashenko, P. Piskorz, I. Komaromi, R. Gomperts, R. L. Martin, M. Challacombe, P. M. W. Gill, B. G. Johnson, W. Chen, M. W. Wong, J. L. Andres, M. Head-Gordon, E. S. Replogle and J. A. Pople, *Gaussian 98 (Revision A.6)*, Gaussian Inc., Pittsburgh, PA, 1998.

33 A. D. Becke, *J. Chem. Phys.*, 1993, **98**, 5648.

34 (*a*) R. Ditchfield, W. J. Hehre and J. A. Pople, *J. Chem. Phys.*, 1971, **54**, 724; (*b*) W. J. Hehre, R. Ditchfield and J. A. Pople, *J. Chem. Phys.*, 1972, **56**, 2257; (*c*) P. C. Hariharan and J. A. Pople, *Theor. Chim. Acta*, 1973, **28**, 213; (*d*) P. C. Hariharan and J. A. Pople, *Mol. Phys.*, 1974, **27**, 209; (*e*) M. S. Gordon, *Chem. Phys. Lett.*, 1980, **76**, 163.

35 J. Tomasi, B. Mennucci and R. Cammi, *Chem. Rev.*, 2005, **105**, 2999–3094.

36 (*a*) L. He, L. Duan, J. Qiao, D. Zhang, L. Wang and Y. Qiu, *Chem. Commun.*, 2011, **47**, 6467–6469; (*b*) F. Kessler,

R. D. Costa, D. Di Censo, R. Scopelliti, E. Ortí, H. J. Bolink, S. Meier, W. Sarfert, M. Gratzel, M. K. Nazeeruddin and E. Baranoff, *Dalton Trans.*, 2012, **41**, 180–191; (*c*) S. B. Meier, W. Sarfert, J. M. Junquera-Hernandez, M. Delgado, D. Tordera, E. Orti, H. J. Bolink, F. Kessler, R. Scopelliti, M. Gratzel, M. K. Nazeeruddin and E. Baranoff, *J. Mater. Chem. C*, 2013, **1**, 58–68; (*d*) E. Baranoff, H. J. Bolink, E. C. Constable, M. Delgado, D. Haussinger, C. E. Housecroft, M. K. Nazeeruddin, M. Neuburger, E. Orti, G. E. Schneider, D. Tordera, R. M. Walliser and J. A. Zampese, *Dalton Trans.*, 2013, **42**, 1073–1087.

37 H. J. Bolink, L. Cappelli, S. Cheylan, E. Coronado, R. D. Costa, N. Lardies, M. K. Nazeeruddin and E. Orti, *J. Mater. Chem.*, 2007, **17**, 5032–5041.

38 E. Margapoti, V. Shukla, A. Valore, A. Sharma, C. Dragonetti, C. C. Kitts, D. Roberto, M. Murgia, R. Ugo and M. Muccini, *J. Phys. Chem. C*, 2009, **113**, 12517–12522.